Обзор ArXiv: astro-ph, 13-19 ноября 2019

От Сильченко О.К.

ArXiv: 1911.05081

The Milky Way's Disk of Classical Satellite Galaxies in Light of Gaia DR2

Marcel S. Pawlowski,[1]★ and Pavel Kroupa[2,3]
[1] *Leibniz-Institut für Astrophysik Potsdam (AIP), An der Sternwarte 16, D-14482 Potsdam, Germany*
[2] *Helmholtz-Institut für Strahlen- und Kernphysik, University of Bonn, Nussallee 14-16, D- 53115 Bonn, Germany*
[3] *Charles University in Prague, Faculty of Mathematics and Physics, Astronomical Institute, V Holešovičkách 2, CZ-180 00 Praha 8, Czech Republic*

Accepted 2019 November 7. Received 2019 November 7; in original form 2019 August 26

ABSTRACT

We study the correlation of orbital poles of the 11 classical satellite galaxies of the Milky Way, comparing results from previous proper motions with the independent data by Gaia DR2. Previous results on the degree of correlation and its significance are confirmed by the new data. A majority of the satellites co-orbit along the Vast Polar Structure, the plane (or disk) of satellite galaxies defined by their positions. The orbital planes of eight satellites align to $< 20°$ with a common direction, seven even orbit in the same sense. Most also share similar specific angular momenta, though their wide distribution on the sky does not support a recent group infall or satellites-of-satellites origin. The orbital pole concentration has continuously increased as more

Name	l [°]	b [°]	$r_\odot$ [kpc]	v_{los} [km s^{-1}]	$\mu_\alpha \cos\delta$ [mas yr^{-1}]	μ_δ [mas yr^{-1}]	$C_{\mu_\alpha,\mu_\delta}$	ϵ_{sys} [mas yr^{-1}]	Type	Ref.
Sgr	5.6	-14.2	26.3	140.0 ± 2.0	−2.650 ± 0.080	−0.880 ± 0.080			Ground†	Ibata et al. (1997)
					−2.830 ± 0.200	−1.330 ± 0.200			Ground	Dinescu et al. (2005)
					−2.750 ± 0.200	−1.650 ± 0.220			HST	Pryor et al. (2010)
					−2.692 ± 0.001	−1.359 ± 0.001	+0.090	0.035	Gaia†	Gaia Collab. et al. (2018)
					−2.736 ± 0.009	−1.357 ± 0.008	+0.114	0.035	Gaia	Fritz et al. (2018b)
LMC	280.5	-32.9	50.6	262.2 ± 3.4	+2.030 ± 0.080	+0.440 ± 0.050			HST	Kallivayalil et al. (2006a)
					+1.956 ± 0.036	+0.435 ± 0.036			HST	Piatek et al. (2008)
					+1.910 ± 0.020	+0.229 ± 0.047			HST†	Kallivayalil et al. (2013)
					+1.850 ± 0.010	+0.234 ± 0.010		0.028	Gaia†	Gaia Collab. et al. (2018)
SMC	302.8	-44.3	64.0	145.6 ± 0.6	+1.160 ± 0.180	−1.170 ± 0.180			HST	Kallivayalil et al. (2006b)
					+0.754 ± 0.061	−1.252 ± 0.058			HST	Piatek et al. (2008)
					+0.772 ± 0.063	−1.117 ± 0.061			HST†	Kallivayalil et al. (2013)
					+0.797 ± 0.010	−1.220 ± 0.010		0.028	Gaia†	Gaia Collab. et al. (2018)
Dra	86.4	34.7	75.9	−291.0 ± 0.1	+0.600 ± 0.400	+1.100 ± 0.500			Ground	Scholz & Irwin (1994)
					+0.177 ± 0.063	−0.221 ± 0.063			HST	Pryor et al. (2015)
					−0.284 ± 0.047	−0.289 ± 0.041			Ground†	Casetti-Dinescu & Girard (2
					+0.056 ± 0.010	−0.176 ± 0.010			HST†	Sohn et al. (2017)
					−0.019 ± 0.009	−0.145 ± 0.010	-0.080	0.035	Gaia†	Gaia Collab. et al. (2018)
					−0.013 ± 0.013	−0.158 ± 0.015	+0.131	0.035	Gaia	Fritz et al. (2018b)
UMi	105.0	44.8	75.9	−246.9 ± 0.1	+0.500 ± 0.800	+1.200 ± 0.500			Ground	Scholz & Irwin (1994)
					+0.056 ± 0.078	+0.074 ± 0.099			Ground†	Schweitzer et al. (1997)
					−0.500 ± 0.170	+0.220 ± 0.160			HST	Piatek et al. (2005)
					−0.182 ± 0.010	+0.074 ± 0.008	-0.340	0.035	Gaia†	Gaia Collab. et al. (2018)
					−0.184 ± 0.026	+0.082 ± 0.023	-0.387	0.035	Gaia	Fritz et al. (2018b)
Scl	287.5	-83.2	85.9	111.4 ± 0.1	+0.720 ± 0.220	−0.060 ± 0.250			Ground	Schweitzer et al. (1995)
					+0.090 ± 0.130	+0.020 ± 0.130			HST	Piatek et al. (2006)
					−0.400 ± 0.290	−0.690 ± 0.470			SRG	Walker et al. (2008)
					+0.030 ± 0.021	−0.136 ± 0.021			HST†	Sohn et al. (2017)
					+0.082 ± 0.005	−0.131 ± 0.004	+0.230	0.035	Gaia†	Gaia Collab. et al. (2018)
					+0.085 ± 0.006	−0.133 ± 0.006	+0.157	0.035	Gaia	Fritz et al. (2018b)
Sxt	243.5	42.3	85.9	224.2 ± 0.1	−0.260 ± 0.410	+0.100 ± 0.440			SRG	Walker et al. (2008)
					−0.409 ± 0.050	−0.047 ± 0.058			Ground†	Casetti-Dinescu et al. (2018
					−0.496 ± 0.025	+0.077 ± 0.020	-0.450	0.035	Gaia†	Gaia Collab. et al. (2018)
					−0.438 ± 0.028	+0.055 ± 0.028	-0.238	0.035	Gaia	Fritz et al. (2018b)
Car	260.1	-22.2	105.2	222.9 ± 0.1	+0.220 ± 0.090	+0.150 ± 0.090			HST†	Piatek et al. (2003)
					+0.250 ± 0.360	+0.160 ± 0.430			SRG	Walker et al. (2008)
					+0.495 ± 0.015	+0.143 ± 0.014	-0.080	0.035	Gaia†	Gaia Collab. et al. (2018)
					+0.485 ± 0.018	+0.132 ± 0.016	+0.083	0.035	Gaia	Fritz et al. (2018b)
Fnx	237.1	-65.7	147.2	55.3 ± 0.1	+0.590 ± 0.160	−0.150 ± 0.160			HST	Dinescu et al. (2004)
					+0.476 ± 0.046	−0.360 ± 0.041			HST†	Piatek et al. (2007)
					+0.480 ± 0.150	−0.250 ± 0.140			SRG	Walker et al. (2008)
					+0.620 ± 0.160	−0.530 ± 0.150			Ground	Méndez et al. (2011)
					+0.376 ± 0.003	−0.413 ± 0.003	-0.090	0.035	Gaia†	Gaia Collab. et al. (2018)
					+0.375 ± 0.004	−0.401 ± 0.005	-0.460	0.035	Gaia	Fritz et al. (2018b)
Leo II	220.2	67.2	233.3	78.0 ± 0.1	+0.104 ± 0.113	−0.033 ± 0.151			HST	Lépine et al. (2011)
					−0.069 ± 0.037	−0.087 ± 0.039			HST†	Piatek et al. (2016)
					−0.064 ± 0.057	−0.210 ± 0.054	+0.050	0.035	Gaia†	Gaia Collab. et al. (2018)
					+0.020 ± 0.090	−0.201 ± 0.093	-0.401	0.035	Gaia	Fritz et al. (2018b)
Leo I	226.0	49.1	253.5	282.5 ± 0.1	−0.114 ± 0.029	−0.126 ± 0.029			HST†	Sohn et al. (2013)
					−0.097 ± 0.056	−0.091 ± 0.047	-0.510	0.035	Gaia†	Gaia Collab. et al. (2018)
					−0.086 ± 0.059	−0.128 ± 0.062	-0.358	0.035	Gaia	Fritz et al. (2018b)

По сравнению с pre-Gaia, в коллектив добавилась Carina

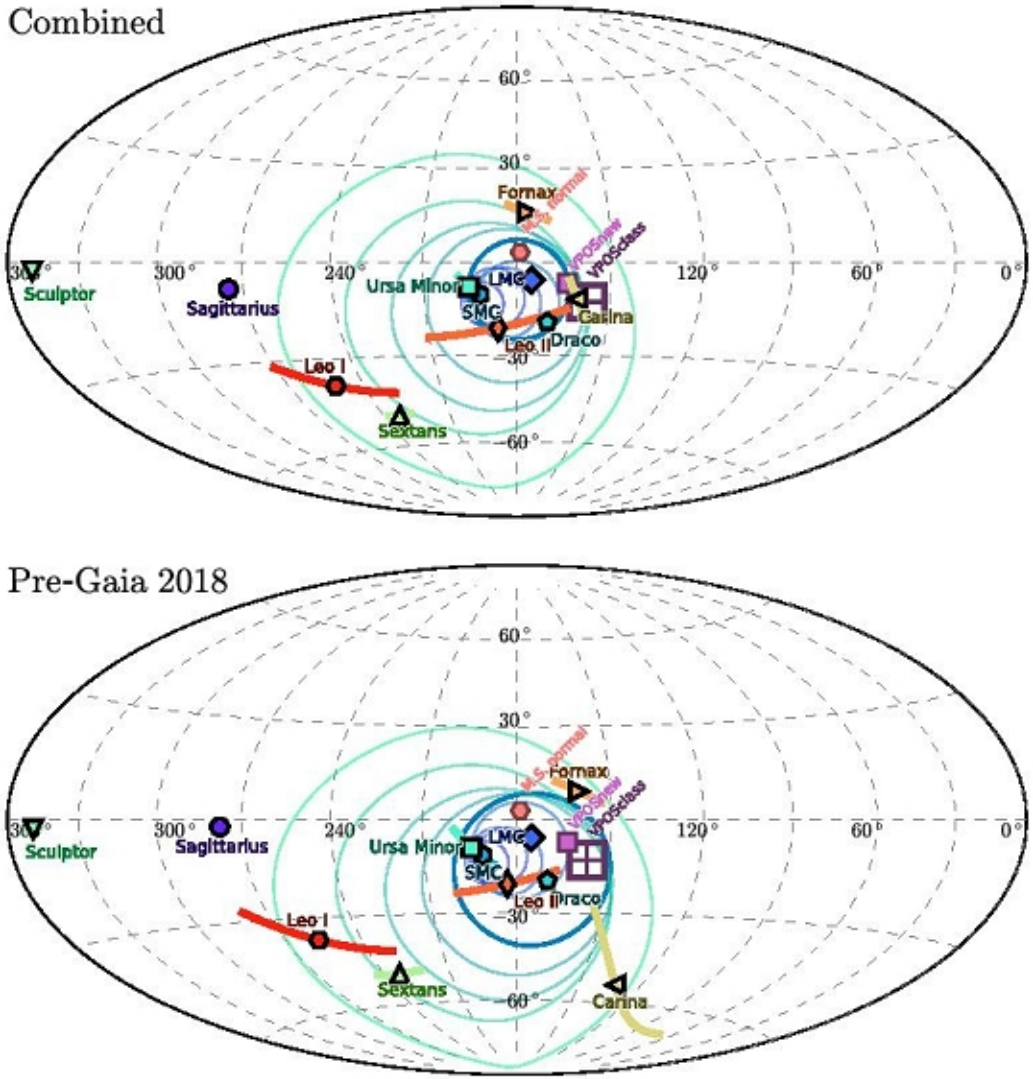

7 спутников вращаются вокруг MW в плоскости в одну сторону

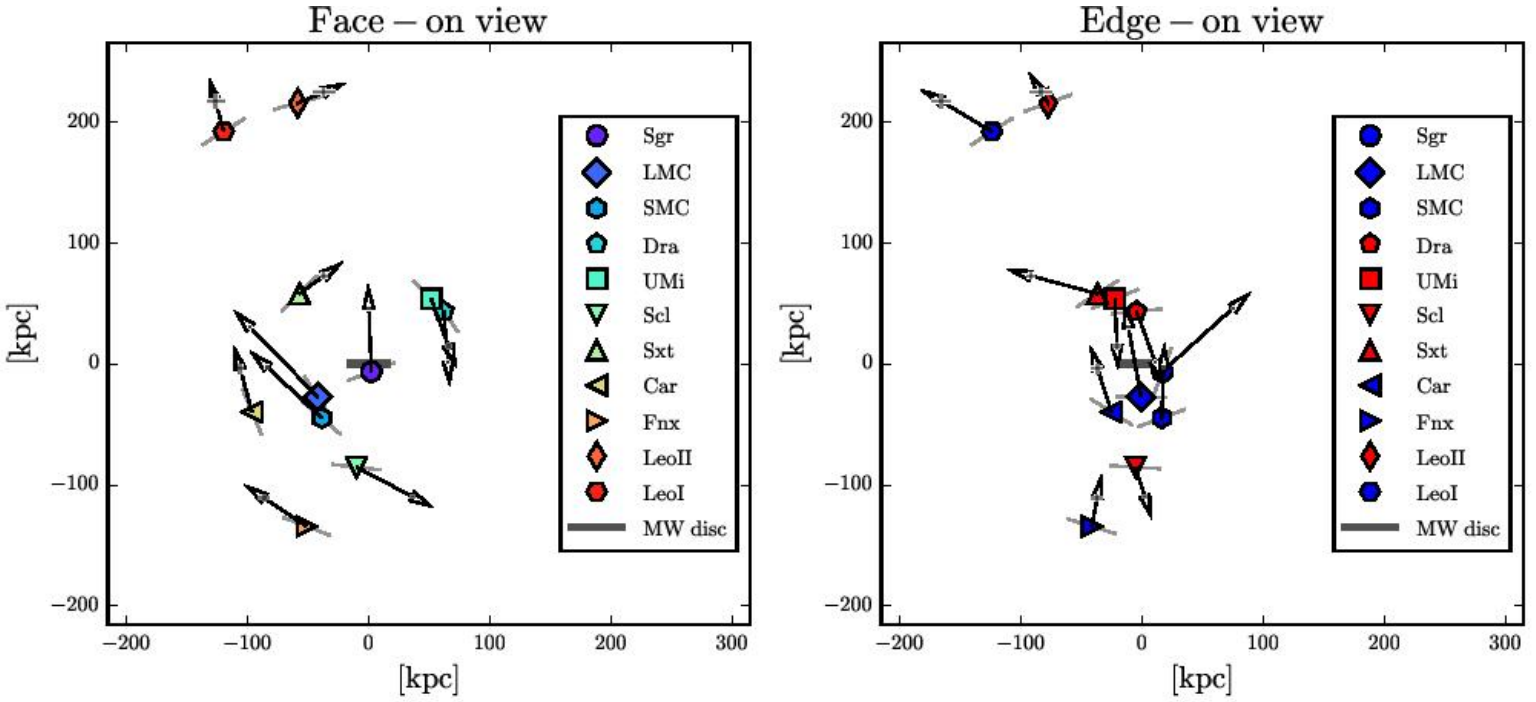

Figure 2. Most-likely 3D velocity vectors of the 11 classical satellite galaxies (black arrows), projected onto a face-on view (left panel) and an edge-on view (right panel) of the average orbital plane determined from the seven best-aligned orbital poles. The absolute lengths of the vectors is arbitrary, but their relative lengths represent the relative velocities of the satellite galaxies. For both panels, the measurement uncertainties in the two plotted velocity components (along the vertical and horizontal axes) are indicated by the grey error bars at the base of the arrow heads. These use the same scale as the velocity vectors. The error bars thus illustrate how little the vectors are allowed to move around within the uncertainties: The errors are generally much smaller than the arrow heads, except for the most distant Milky Way satellites. The grey lines indicate the tangential direction at each satellite's position. Most satellites have highly tangentially biased velocites in the face-on view, but much more radial velocities in the edge-on view. With the exception of Leo I, Sextans, and Sagittarius, the classical satellites of the Milky Way thus move predominantly in a common plane. In the edge-on view (right panel) the satellites are color-coded according to their line-of-sight velocity: red for receding, blue for approaching in this

Сравнение с изотропной выборкой из Монте-Карло

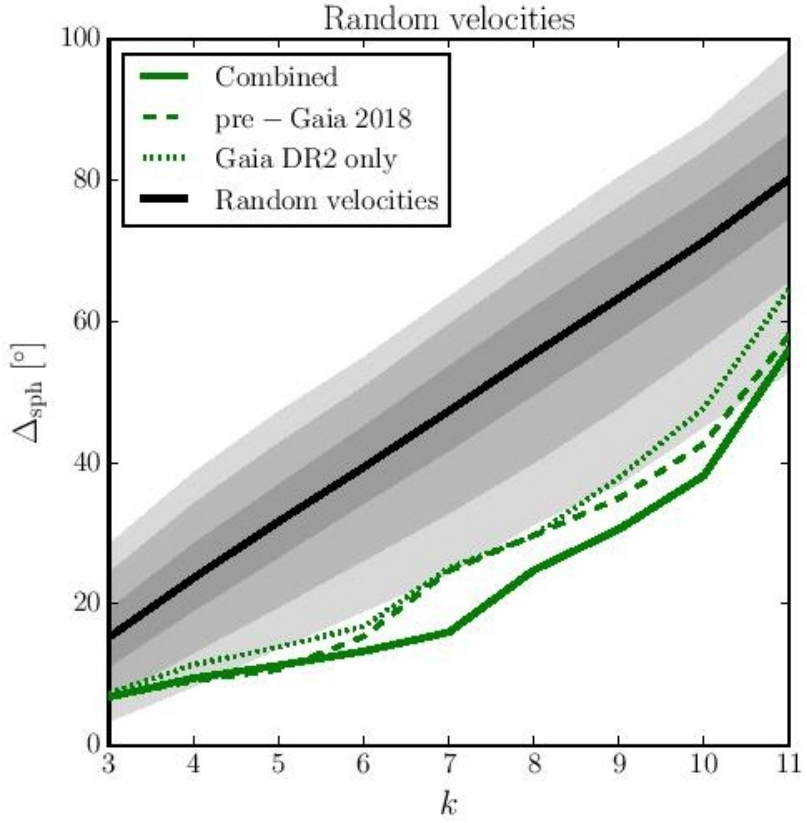

Figure 4. Comparison of the spherical standard distances $\Delta_{\rm std}$ of the k most-concentrated orbital poles with the expected distribution from 2500 realizations of random velocity vectors drawn from isotropy of the classical satellites (but fixed observed 3D positions). The three observational proper motion samples are shown as green lines. Contours on the model distribution indicate regions containing 50, 90 and 99 per cent of all realizations.

Но все-таки плоскость не бесконечно тонкая: толщина ~20 кпк

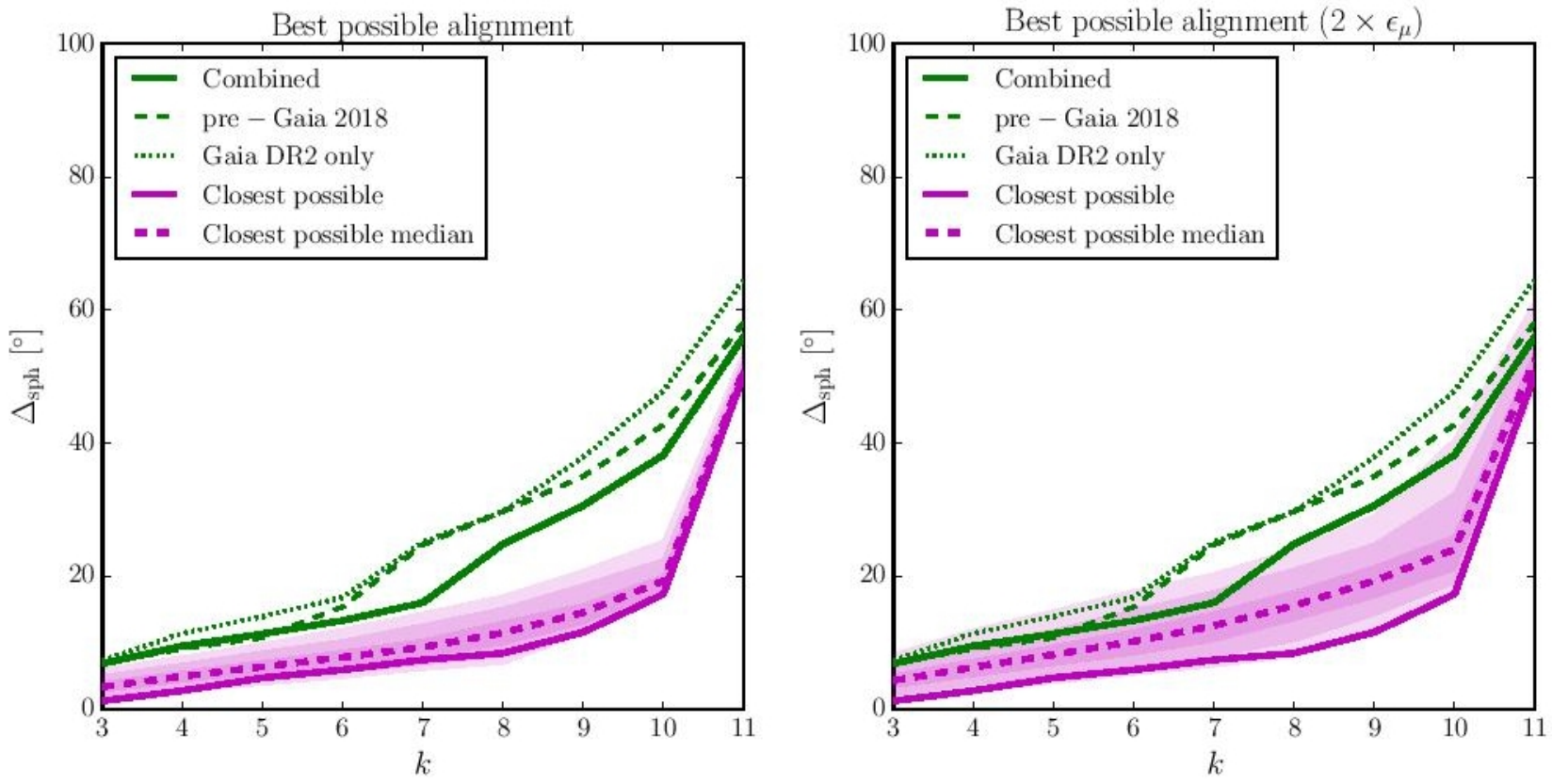

Figure 6. Same as Fig. 4, but comparing to the orbital pole directions that best align with the normal to the VPOSclass. The solid magenta line gives the standard distances for the best-aligned poles, while the dashed line and the shaded regions are derived from 2500 realizations of mock-observing this while accounting for proper motion uncertainties of $\epsilon_\mu = 0.05\,\mathrm{mas\,yr^{-1}}$ (left panel) and $\epsilon_\mu = 0.1\,\mathrm{mas\,yr^{-1}}$ (right panel).

Сравнение с LCDM последней модели

We use the Illustris TNG project, specifically the hydrodynamical simulation TNG100-1 and its dark-matter-only equivalent TNG100-1-Dark (Naiman et al. 2018; Springel et al. 2018; Marinacci et al. 2018; Nelson et al. 2018; Pillepich et al. 2018). The simulation has a box size of 75Mpc/h at $z = 0$ and a dark matter particle mass of $m_{\rm DM} = 7.5 \times 10^6\ M_\odot$ ($m_{\rm DM} = 8.9 \times 10^6\ M_\odot$ for TNG100-1-Dark). This provides a good compromise between simulation volume (to ensure a sufficiently large sample of potential host galaxies with masses comparable to that of the Milky Way), and resolution (so that most of the selected hosts in the Milky Way mass range are indeed surrounded by at least 11 subhalos). The adopted cosmological parameters of Illustris TNG are consistent with Planck Collaboration et al. (2016). We use the publicly available redshift zero galaxy catalogs (Nelson et al. 2019).

4.1 Selection and analysis of simulated satellite systems

As potential Milky Way analogues, we first select all halos with a total mass M_{200} of 0.5 to $2.0 \times 10^{12}\ M_\odot$ within a sphere containing a mean density of 200 times the critical density of the universe at $z = 0$. There are 2660 halos in this mass range in TNG100-1. Furthermore, to ensure a sufficient isolation,

Сравнение с LCDM последней модели только по орбитам

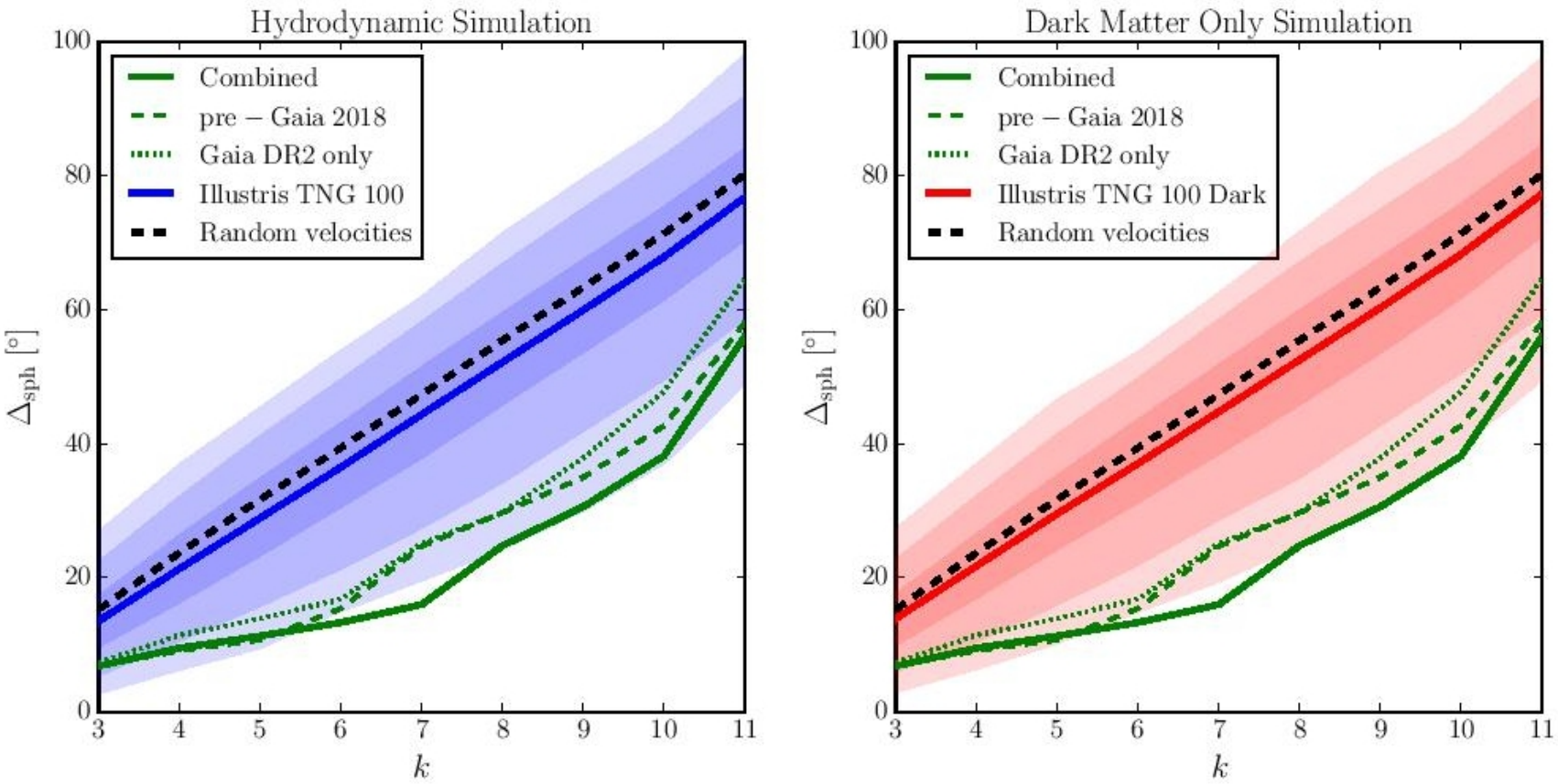

Figure 8. Same as Figs. 4 and 6, but comparing to the distribution of orbital pole directions derived from the hydrodynamical Illustris TNG100-1 cosmological simulation (left panel) and its dark matter only equivalent TNG100-1-Dark (right panel). For comparison, the median $\Delta_{\rm std}$ from the random velocities (black solid line in Fig. 4) is shown as a black dashed line.

ArXiv: 1911.05039

ORIGINAL PAPER

Helium abundance (and H_0) in X-COP galaxy clusters

S. Ettori*[1,2] | V. Ghirardini[3] | D. Eckert[4]

[1] INAF, Osservatorio di Astrofisica e Scienza dello Spazio, via Pietro Gobetti 93/3, 40129 Bologna, Italy
[2] INFN, Sezione di Bologna, viale Berti Pichat 6/2, I-40127 Bologna, Italy
[3] Center for Astrophysics | Harvard & Smithsonian, 60 Garden Street, Cambridge, MA 02138, USA
[4] Department of Astronomy, University of Geneva, Ch. d'Ecogia 16, CH-1290 Versoix, Switzerland

Correspondence
*Corresponding author; Email: stefano.ettori@inaf.it

We present the constraints on the helium abundance in 12 X-ray luminous galaxy clusters that have been mapped in their X-ray and Sunyaev-Zeldovich (SZ) signals out to R_{200} for the *XMM-Newton* Cluster Outskirts Project (X-COP). The unprecedented precision available for the estimate of H_0 allows us to investigate how much the reconstructed X-ray and SZ signals are consistent with the expected ratio x between helium and proton densities of 0.08–0.1. We find that a H_0 around 70 km s^{-1} Mpc^{-1} is preferred from our measurements, with lower values of H_0 as requested from the Planck collaboration (67 km s^{-1} Mpc^{-1}) requiring a 34% higher value of x.

KEYWORDS:
galaxies: clusters: general – X-rays: galaxies: clusters – (galaxies:) intergalactic medium – (cosmology:) cosmological parameters

Если сопоставить рентген и эффект Сюняева-Зельдовича, то можно огранить комбинацию обилия гелия и постоянной Хаббла

$\epsilon \propto n_e n_p(1+4x) \sim n_p^2(1+4x)(1+2x)$, where the relation $n_e/n_p = 1+2x$ holds. This approximation is reasonable because the contribution from other metals with atomic number $Z_i \geq 3$ raises the value of $(1+4x)(1+2x)$ by about 3%.

Hence, for an observed X-ray flux $f \propto \epsilon R^3/d_L^2$, n_p scales as $h^{0.5}[(1+4x)(1+2x)]^{-0.5}$, where d_L is the luminosity distance that is proportional to the Hubble constant h^{-1}, and R is the proper radius equal to the angular scale times the angular diameter distance $d_A = d_L/(1+z)^2$.

The X-ray pressure is the product of the spectral measurement of the gas temperature, T_e, by the electron density n_e estimated by the geometrical deprojection of the observed surface brightness $S_X \propto \int n_e n_p(1+4x)dl$, that implies the following scaling:

$$n_{e,X} \sim \mathrm{deproj}(S_X)^{0.5}\left(\frac{1+2x}{1+4x}\right)^{0.5} h^{0.5}. \quad (3)$$

The SZ pressure is obtained directly from the deprojection of the Compton parameter $y \propto \int n_e T_e\, dl$:

$$(n_e T_e)_{SZ} \sim \mathrm{deproj}(y)\, h. \quad (4)$$

X=n(He)/n(H)

Under the assumption of spherical symmetry, and that the gas density reconstructed from X-ray is not affected from clumpiness (e.g. Nagai & Lau, 2011; Roncarelli et al., 2013) that might bias high its value, we can write the ratio between the two estimates of the pressure as

$$\frac{P_{SZ}}{P_X} = \frac{(n_e T_e)_{SZ}}{n_{e,X} T_e} \sim \left(\frac{1+4x}{1+2x}\right)^{0.5} h^{0.5} = \eta. \quad (5)$$

Данные наблюдений

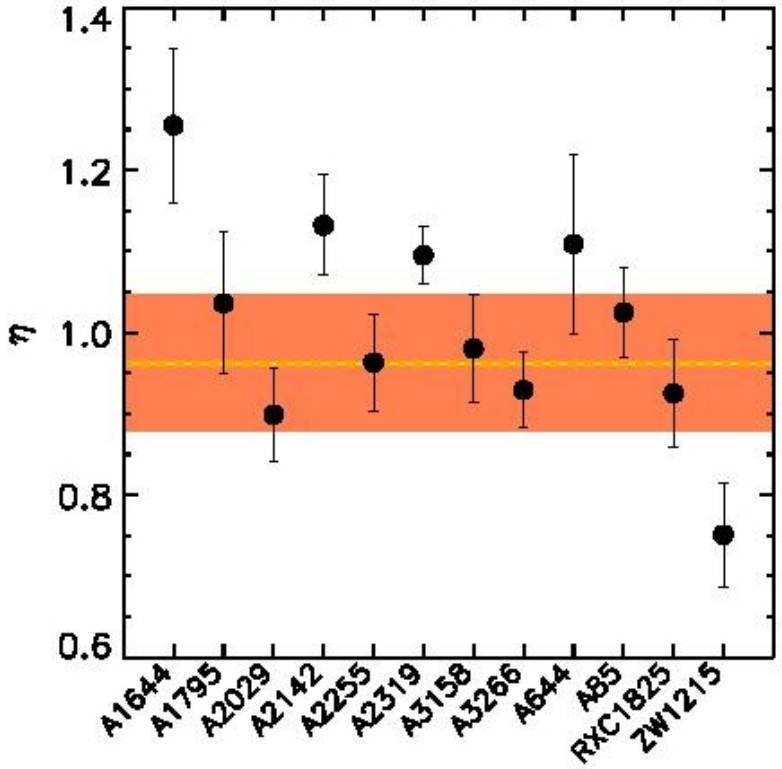

FIGURE 3 Result on the parameter $\eta = P_{SZ}/P_X$ obtained from a best-fit of the pressure profiles for each X-COP object. The coloured areas indicate the scatter (0.0838) in the distribution and the error (0.0013) on the central position of the joint-fit value $\eta_{X-COP} = 0.9624$, used in the present analysis.

Результаты (ограничения) для обилия гелия и постоянной Хаббла

3.2 | $\eta + H_0$: results on x

From the measurements of η obtained in the X-COP sample and the adopted values of H_0 (see subsection 2.1), we can use Equation 5 to estimate $\theta = \eta^2/h$. We show the constraints on θ in Fig. 4 . Low values of x, lower than the one (*angr*) adopted in the X-COP X-ray analysis seem to be preferred from high values of the Hubble constant. In particular, for $H_{0,LMC}$ (74 km s^{-1} Mpc^{-1}), $x = 0.055 \pm 0.013$, whereas for $H_{0,CMB}$ (67.4 km s^{-1} Mpc^{-1}), $x = 0.131 \pm 0.008$. These values should be compared with a cosmic value of $x_{BBN} = 0.0869$ and $x = 0.0977$ for the abundance table in *angr*.

Reversely, fixing x equal to the values from BBN, *aspl*, *angr*, we measure $H_0 = 70.9, 71.0, 69.9$ km s^{-1} Mpc^{-1},

<-- если зафиксировать гелий как первичный